Invited Paper

Transparent metals and inhomogeneous meta-surfaces

Zhengyong Song, Shiyi Xiao, Qiong He, Shulin Sun, and Lei Zhou *
State Key Laboratory of Surface Physics, Key Laboratory of Micro and Nano Photonic Structures (Ministry of Education) and Physics Department, Fudan University, Shanghai 200433, China
* Email: phzhou@fudan.edu.cn

(Received May 2, 2013)

Abstract: We present a short overview on the research works related to two hot topics in metamaterials: transparent metals and inhomogeneous meta-surfaces. For the first topic, we first introduce a scattering-cancellation mechanism for making continuous metals optically transparent, and then propose a realistic design in optical domain, and finally experimentally prove the idea in both microwave and terahertz frequency domains. For the second topic, we show that light reflection/refraction at a carefully designed gradient-index meta-surface follows a generalized Snell's law, and then demonstrate that such a system can perfectly convert a propagating electromagnetic wave to a surface wave under certain conditions, and finally introduce several interesting applications of this type of systems.

Keywords: Metamaterials, Transparent metal, Terahertz, Scattering cancellation mechanism.

1. Introduction

Metamaterials (MTMs) are artificial electromagnetic (EM) materials composed by functional EM microstructures (usually called "meta-atom") arranged in a specific macroscopic order. Via changing their constitutional meta-atoms or macroscopic orders, MTMs can exhibit extraordinary EM properties which do not exist in nature. The most remarkable properties of MTMs are that they can be designed to manipulate EM wave propagation properties as desired, leading to many interesting phenomena already demonstrated, such as negative refraction [1, 2], super imaging [3, 4], invisibility cloaking [5, 6] and polarization control [7, 8].

Recently, much attention was paid to two sub-fields in MTM research. On the one hand, people were fascinated to seek for new routes to make transparent conducting metals (TCMs) based on MTMs, particularly those schemes that can make *continuous* metals optically transparent so as to keep the highest possible conductivity of a target metal. Meanwhile, people gradually realized the importance of macroscopic "order" of a MTM to control the wave-front of light, and found that a class of inhomogeneous meta-surfaces (i.e., ultra-thin MTMs) possesses extraordinary abilities to control light propagations. In this paper, we attempt to make a brief review on the latest developments in these two hot topics, mainly focusing on the research works

done in our own group. This paper is by no means a complete overview on the whole developments of these two fields, but rather represents our own perspectives and serves as a guidance to help readers enter these two sub-fields.

This paper is organized in the following way. Section 2 is devoted to reviewing the TCM part. We first give a brief introduction on the background and motivation of the given problem in Sec. 2.1, and then introduce in Sec. 2.2 our concept of scattering cancellation mechanism to achieve TCM. We next describe our efforts to experimentally prove this concept in both microwave and terahertz (THz) frequency domains in Secs. 2.3 and 2.4, respectively. Section 3 is devoted to reviewing the meta-surface part, in which we summarize the key idea of the generalized Snell's law, the implementations of this idea in different frequency domains and the applications of such devices. Finally, we conclude this review in Sec. 4.

2. Transparent conducting metals based on MTMs

2. 1 Backgrounds and motivations

Making a high-conducting metal transparent has drawn lots of attention recently. The problem is of great scientific curiosity since a bare metal itself is opaque for light. On the application side, TCMs with both high DC conductivity (σ_{DC}) and high light transmission are desired in optoelectronic devices，varying from solar cells to electronic paper, touch screens, and displays. However, since $\sigma_{DC} = n_e e^2 \tau / m$ of a metal is correlated with its plasmon frequency $\omega_p^2 = n_e e^2 / \varepsilon_0 m$ through the free-electron density n_e, a high-conducting metal (with a high n_e) is typically opaque for light since its permittivity ε is usually very negative caused by its high ω_p. Typical approaches to fabricate TCMs are to decrease the n_e directly (e.g., using Indium-Tin-Oxide (ITO) [9] or doped silicon [10]) or effectively (e.g., making nano-meshes [11] or nano-wires [12]). However, the (effective) DC conductivity (σ_{DC}) of such TCMs are much smaller than that of a continuous metal film [13]. Meanwhile, ITO is very brittle thus making devices like electronic paper or flexible screens difficult to achieve [14], not mentioning the scarcity and continuous increase in the price of indium. On the other hand, transparency of a metal film can also be achieved with help of certain resonances such as surface plasmon polaritons (SPP) [15] or Fabry-Perot (FP) resonances [16]. However, in such schemes, the targeted metals should be perforated with holes or slits. Moreover, the SPP approach is sensitive to structural order while the FP one requires samples with thicknesses comparable to wavelength, both of which are undesired in practical applications. Therefore, it is highly desirable to find a new mechanism to make a *continuous* plasmonic metal optically transparent.

2.2 The scattering cancellation mechanism

In 2005, we proposed the concept of SCM [17], which is different from previous SPP-aided [15] or FP ones [16], to make a continuous and flat metal transparent. Our idea is motivated by effective medium theory (EMT) [18]. Let us consider a homogeneous layer B of thickness d_2 with $\varepsilon_2 < 0$, which represents a continuous plasmonic metal and by itself is optically opaque. Consider first a double layer structure combining this layer with another homogeneous layer A with $\varepsilon_1 > 0$ and thickness d_1. Within the effective medium framework, the AB structure will become transparent when $\bar{\varepsilon} = (\varepsilon_1 d_1 + \varepsilon_2 d_2)/(d_1 + d_2) = 1$. For a circular frequency ω and fixed parallel **k** component $k_{\parallel}$, we obtain a 2×2 transfer matrix $Q(\omega, k_{\parallel})$, by which both the transmission coefficient $t = Q_{11} - Q_{12}Q_{21}/Q_{22}$ and reflection coefficient $r = -Q_{21}/Q_{22}$ can be calculated [19]. If there is no absorption, perfect transmission ($T = |t|^2 = 1$) appears when $Q_{21} = 0$. For this AB structure, the criterion of perfect transmission at normal incidence ($k_{\parallel} = 0$) is:

$$(\frac{k_1}{k_0} - \frac{k_0}{k_1})\tan(k_1 d_1) - (\frac{\alpha_2}{k_0} + \frac{k_0}{\alpha_2})\tanh(\alpha_2 d_2) + i(\frac{k_1}{\alpha_2} + \frac{\alpha_2}{k_1})\tan(k_1 d_1)\tanh(\alpha_2 d_2) = 0 \qquad (1)$$

where $k_l = \sqrt{\varepsilon_l}\,\frac{\omega}{c}$ and $k_2 = i\alpha_2$. Since the first two terms are real while the third term is imaginary, Eq. (1) can never be satisfied, indicating that perfect transmission cannot be realized in the AB structure. The reason is that the waves scattered by layers A and B cannot completely cancel each other, since the two layers are in different phase planes. This problem can be remedied when another identical A layer is added to form an ABA sandwich structure. For this structure, we found the following rigorous criterion for perfect transmission:

$$(\frac{k_1}{k_0} - \frac{k_0}{k_1})2\tan(k_1 d_1) - (\frac{\alpha_2}{k_0} + \frac{k_0}{\alpha_2})\tanh(\alpha_2 d_2) - (\frac{k_1^2}{\alpha_2 k_0} + \frac{\alpha_2 k_0}{k_1^2})\tan^2(k_1 d_1)\tanh(\alpha_2 d_2) = 0, \qquad (2)$$

The third term in the above equation is also real so that Eq. (2) can be satisfied with appropriate parameter values. This perfect transmission is not induced by SPP's, since the latter correspond to the condition $Q_{22}(\omega, k_{\parallel}) = 0$ [20], while the present criterion is $Q_{21}(\omega, k_{\parallel}) = 0$. The present transparency is also not induced by FP interference, since no propagating wave is allowed inside our B layer.

The first two terms in Eq. (2) are single scattering contributions of individual A and B layers, while the third term is a multiple scattering contribution. In the long wavelength limit ($k_i d_i \to 0$), the third term can be dropped and Eq. (2) is reduced to the EMT solution:

$\bar{\varepsilon} = (2\varepsilon_1 d_1 + \varepsilon_2 d_2)/(2d_1 + d_2) = 1$. However, when $k_1 d_1$ and $\alpha_2 d_2$ are not small, Eq. (2) still has solutions. Figure 1(a) shows the solved values of ε_1 as a function of d_2 for an example with $\varepsilon_2 = -2000$. To avoid the confusion of too many parameters, we set $d_1 = d_2 = d$. We find the existence of two solutions up to a critical thickness at which the solutions merge together and disappear abruptly. The first solution recovers the EMT value in the limit of $k_0 d \to 0$, but at the critical thickness, we have $k_1 d \approx 1.3, \alpha_2 d \approx 2.7$, far away from the long-wavelength limit requirement. The first solution deviates from the EMT value with increasing d, although it is derived from the EMT. A ε_2 : d phase diagram is shown in Fig. 1(b) for this EMT-derived solution ε_1, scaled by its corresponding EMT value. A phase boundary is found to separate the lower-left region which supports the $T = 1$ solutions from the upper-right one which does not. The solution is closer to the EMT value in regions closer to the lower-left corner where EMT is better applicable. However, $T = 1$ solutions survive when EMT is apparently no longer valid.

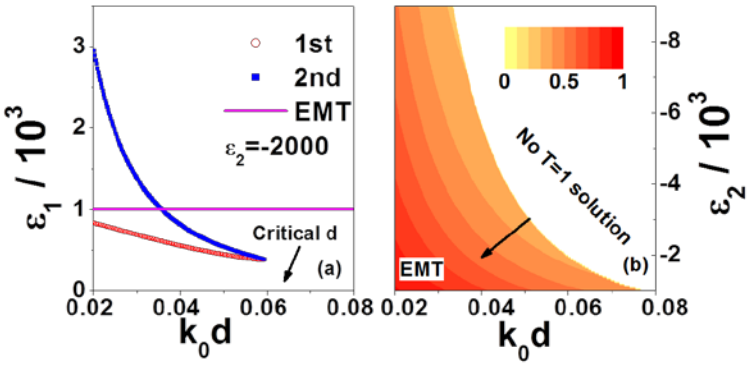

Fig. 1 (color online) (a) ε_1 satisfying Eq. (2) as functions of d. Magenta line denotes the EMT solution $\varepsilon_{EMT} = 3/2 - \varepsilon_2/2$. (b) ε_2 : d phase diagram depicting the value of $\varepsilon_1/\varepsilon_{EMT}$ for the EMT-derived perfect transmission solution. Reproduced from Ref. [17].

Figures 2(a)-(b) shows the field patterns for the two $T = 1$ solutions. In both cases, we find exponentially growing evanescent waves inside the B layer to completely compensate the usual exponentially decaying wave, resulting in perfect transmissions. We find the magnetic fields to be strongly enhanced around the A/B interfaces, which is a characteristic feature of this phenomenon but not found in others. On the other hand, the electric field is diminished inside the B layer. After considering the phase (not shown here), we find the magnetic field pattern to exhibit odd symmetry with respect to the center plane of layer B for the EMT-derived solution, and even symmetry for the second solution. A phase diagram is given in Fig. 2(c) to show the maximum enhancement of magnetic field with respect to parameters ε_2 and $d(=d_1=d_2)$ for the EMT-derived transmission. The field enhancement is stronger with larger ε_2 and appropriate d, in clear contrast to the EMT applicable region shown in Fig. 1(b). This indicates that the high magnetic field is not a natural consequence of EMT.

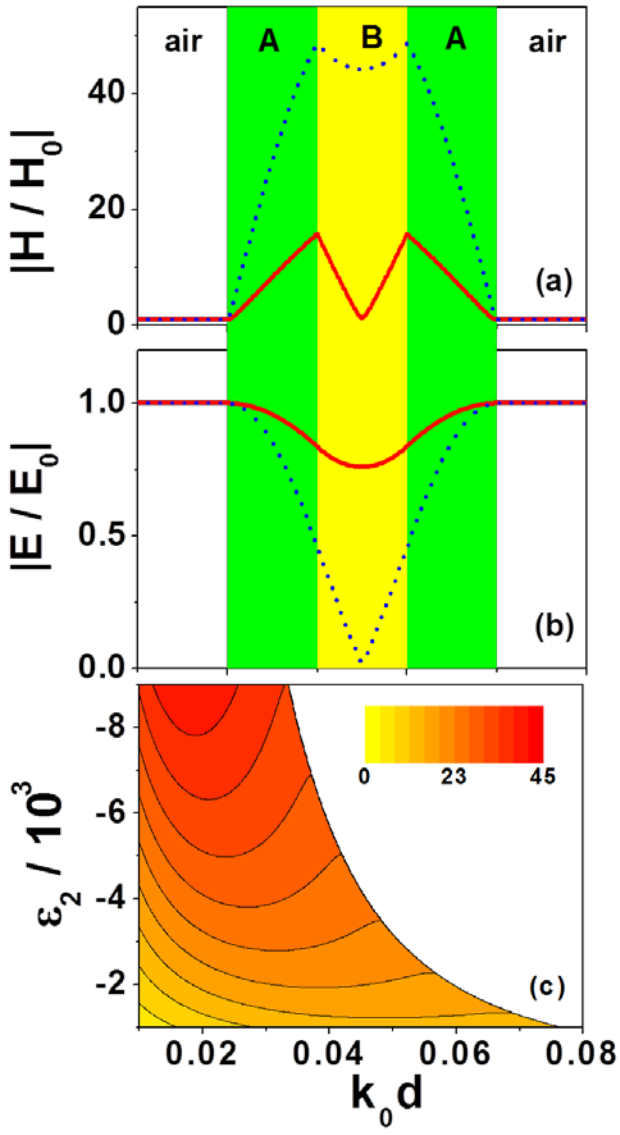

Fig. 2 (color online) $|H/H_0|$ (a) and $|E/E_0|$ (b) as the functions of position for the EMT-derived solution (Solid) and the other solution (dashed). Here $\varepsilon_2 = -2000, k_0 d = 0.02$. (c) Maximum magnetic field enhancement obtained in the EMT-derived perfect transmission state with respect to ε_2 and d. Reproduced from Ref. [17].

2.3 Practical designs for TCMs in optical regime

In principle, the SCM established in Sec. 2.2 can be realized in any frequency domain if one can find those slabs with appropriate permittivity. While required high-permittivity medium can be achieved with MTMs in low-frequency regime (e.g., *GHz*) [17], a direct scaling of those MTMs to optical regime is proven invalid because of the saturation effect of the LC-resonance [21]. In optical frequency domain, it is thus very difficult to employ the conventional MTM concept to obtain a desired high-permittivity slab to make the SCM work.

To solve this problem, we proposed a modified SCM [22], which can work in the visible regime, to make a *continuous* metal film perfectly transparent. Figure 3(a) schematically depicts our proposed structure, in which the target continuous metal film C (with thickness h_C and relative permittivity ε_C) is sandwiched by two identical composite layers (with thickness h_{AB}) consisting of alternate dielectric (A) and metallic (B) stripes. To avoid electric shorting, C layer is separated from AB layers by small gaps (with thicknesses h_a) filled with a medium with relative permittivity ε_a. As a pure theoretical model, we set $\varepsilon_C = -110$ and performed full-wave simulations based on the finite-element-method (FEM) [23] to compute the transmittance (T) of the whole structure under illuminations of an x-polarized normally incident light. We depicted in Fig. 3(b) how T depends on two parameters ε_B and $P = w_A + w_B$ (through varying w_A only), with other parameters fixed as $\varepsilon_A = 12$, $w_B = 0.1\lambda$, $h_{AB} = h_C = 0.02\lambda$, $\varepsilon_a = 1$, $h_a = 0.01\lambda$ where λ is the incident wavelength. Although a standing-alone C layer is nearly opaque (with $T < 2\%$), we note that such a sandwich structure can be perfectly transparent under certain conditions. The upper high-T band at $P \sim \lambda$ is very narrow, and is easily identified as the SPP-aided extraordinary optical transmission (EOT) [15]. The lower high-T band is much broader, with governing physics explained below.

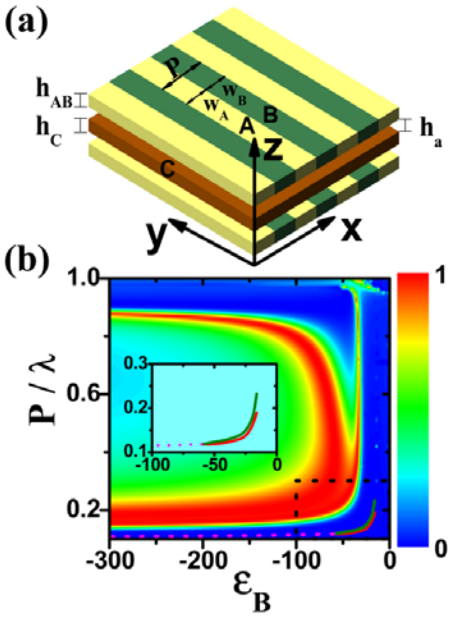

Fig. 3 (color online) (a) Geometry of proposed TCM in the visible regime. (b) FEM calculated transmittance through the structure as functions of ε_B and P/λ. Solid lines represent the solutions of Eq. (1) and the dashed line represents the maximum-transmission solutions obtained with the analytical model. Inset shows a zoomed view of the rectangular region. Reproduced from Ref. [22].

We applied a mode-expansion theory [24, 25] to analytically solve the scattering problem of the present system under two approximations. First, we retain only the zero-order diffraction

modes in air regions, and only the fundamental Bloch modes inside the two periodic AB layers. Second, we homogenize layer C plus two tiny gaps as an effective medium with a volume-averaged $\bar{\varepsilon}_C$ and a modified thickness $\bar{h}_C = h_C + 2h_a$. The first approximation is well justified for the lower high-T band since $P << \lambda$, and the second is also reasonable since $h_C,\ h_a << \lambda$. With material loss neglected in the model, perfect transparency is equivalent to zero reflection, leading to the following equation:

$$\begin{aligned}&\left(\frac{Z_0}{Z_{AB}} - \frac{Z_{AB}}{Z_0}\right) 2\tan(k_{AB}^z h_{AB}) - \left(\frac{\alpha_C}{k_0} + \frac{k_0}{\alpha_C}\right)\tanh(\alpha_C \bar{h}_C) \\ &- \left(\frac{\alpha_C Z_{AB}^2}{k_0 Z_0^2} + \frac{k_0 Z_0^2}{\alpha_C Z_{AB}^2}\right)\tan^2(k_{AB}^z h_{AB})\tanh(\alpha_C \bar{h}_C) = 0\end{aligned}, \tag{3}$$

where $k_0 = \omega / c,\ Z_0 = \sqrt{\mu_0} / \sqrt{\varepsilon_0},\ \alpha_C = \sqrt{|\bar{\varepsilon}_C|}k_0$. k_{AB}^z is obtained by solving the Bloch mode equation of the AB structure (setting Bloch wavevector $K_x = 0$),

$$2\cos(k_A^x w_A + k_B^x w_B) - \left(\frac{\varepsilon_B k_A^x}{\varepsilon_A k_B^x} + \frac{\varepsilon_A k_B^x}{\varepsilon_B k_A^x} - 2\right)\sin(k_A^x w_A)\sin(k_B^x w_B) = 2, \tag{4}$$

in which both k_A^x and k_B^x are implicit functions of k_{AB}^z : $k_B^x = \sqrt{\varepsilon_B k_0^2 - (k_{AB}^z)^2}$, $k_A^x = \sqrt{\varepsilon_A k_0^2 - (k_{AB}^z)^2}$. Z_{AB} is the effective impedance of the AB layer which is given by

$$Z_{AB} = Z_0 k_{AB}^Z S_E / (k_0 S_H), \tag{5}$$

where

$$S_H = P^{-1}\int_0^P H_y^{(0)}(x)dx,\ S_E = P^{-1}\left[\int_0^{w_A} \varepsilon_A^{-1} \cdot H_y^{(0)}(x)dx + \int_{w_B}^P \varepsilon_B^{-1} \cdot H_y^{(0)}(x)dx\right], \tag{6}$$

are two overlapping integrals between incident wave and the fundamental Bloch mode inside the AB layer (with eigen wavefunction described by $H_y^{(0)}(x)$). We numerically solved Eq. (3) for the present structure, and depicted the obtained perfect transparency solutions in Fig. 3(b) by two solid lines. As $\varepsilon_B < -60$, Eq. (3) ceases to have perfect transparency solutions, but we can still find the high-transmission solutions by minimizing the reflections from the entire system (denoted by the dashed line in Fig. 3(b)). The analytical results well reproduced all salient features of the lower high-T band, although quantitative deviations do exist due to neglecting the higher-order contributions in our theory.

The analytical model established a clear picture for the noted transparency. The first two terms in Eq. (3) can be understood as the reflections from individual AB layers and C layer, while the third term represents the multiple scattering effects. While the C layer is always highly reflective [see the 2nd term in Eq. (3)], if the reflection from the AB layer [the 1st term in Eq. (3)] is strong enough to cancel the reflection from the C layer, the whole structure can still be perfectly transparent. For this to be true, we need a mechanism to tune the scatterings from the two AB layers. Since ε_A and ε_B have opposite signs, Eq. (6) shows that the two terms in S_E can largely cancel each other so that S_E can be made very small. Therefore, via adjusting the AB structure one can tune the effective impedance Z_{AB} very efficiently, and in turn, to tune the scatterings from two AB layers so that Eq. (3) can be exactly satisfied under certain conditions. Obviously, such a SCM needs not structuring the metal C, so that full DC conductivity of metal C can be retained. We note that the SCM band is very broad and becomes almost independent on P in the region $-90 < \varepsilon_B < -30$, indicating that such a transparency is robust against structure disorder, a character that many other transparency schemes do not possess.

We designed realistic TCMs based on Fig. 3(a) in which both C and B are assumed as Ag, material A is set as air and the spacers between AB and C are assumed as Al_2O_3. Figure 4(a) presents the FEM calculated transmission spectra for two of our designs, with silver described by a Drude model $\varepsilon_{Ag} = 5 - \omega_p^2 / \omega(\omega + i\Gamma)$ with $\omega_p = 1.37 \times 10^{16}$ Hz and $\Gamma = 2.73 \times 10^{13}$ Hz according to Ref. [26]. For the $h_C = 40$ *nm* design, we found $T \sim 75\%$ at ~700 *nm* which is remarkable since the T through a bare C layer is less than 3%. The T at 776 *nm* is enhanced to 90% with a much larger bandwidth for the $h_C = 25$ *nm* design. There are other models in literature [27, 28] to describe ε_{Ag}, which adopted Γ values 3-4 times larger than ours. We took those models to re-perform the calculations, and found that the qualitative transparency behaviors did not change.

We emphasize that these designs are practically realizable with current technology, particularly noting the recent exciting achievements in multilayer fabrications [29]. Via changing w_B from 50 *nm* to 150 *nm* with $w_A = 50$ *nm* fixed, we show in Fig. 4(b) that the transparency wavelength changes from 700 *nm* to 1600 *nm*, demonstrating the flexibility of our design. We plotted in Fig. 4(c) the distributions of H-field and the energy flux inside the $h_C = 40$ *nm* structure studied in Fig. 4(a), right at $\lambda = 726$ *nm*. Clearly, the incident photons are squeezed into material A and then coupled through layer C aided by strongly enhanced H fields localized in the gaps between B and C. Figure 4(c) showed that the second AB layer played an important role to make the SCM work. In fact, with only one AB layer attached to the C layer, the whole structure is much less transparent but strongly absorb light instead, resembling recently realized optical absorbers [30]. In addition, replacing the Ag stripes by Ag patches, we found an isotropic TCM working for both $\vec{E} \parallel \hat{x}$ and $\vec{E} \parallel \hat{y}$ polarizations. Similar structures have also been proposed by

Hao *et al*., but are operated based on another mechanism [31].

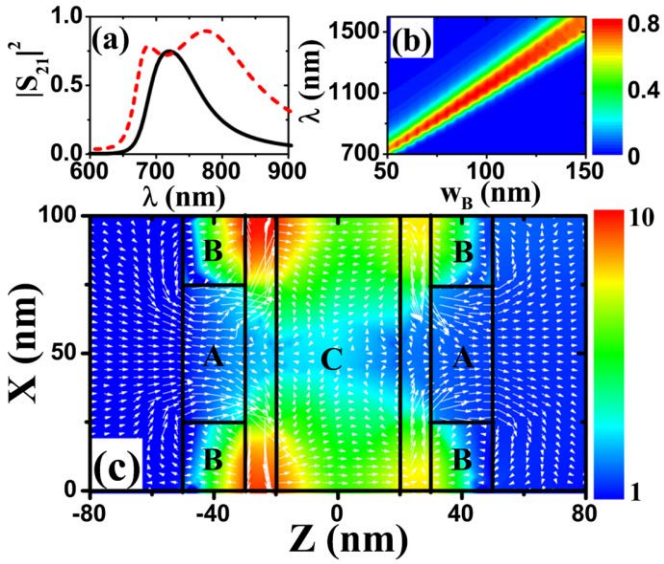

Fig. 4 (color online) (a) FEM calculated transmission spectra of the designed TCMs (solid line for $h_C = 40\ nm$ and dashed line for $h_C = 25\ nm$) with other parameters $\varepsilon_A = 1,\ \varepsilon_a = 3.06,\ w_A = w_B = 50\ nm,\ h_{AB} = 20\ nm,$ and $h_a = 10\ nm$. (b) Transmittance through the $h_C = 40\ nm$ structure as functions of wavelength λ and the width w_B of metallic stripe. (c) Distributions of normalized H-field (color-map) and energy flux (arrows) inside the $h_C = 40\ nm$ structure under the illumination of an x-polarized light at $\lambda = 726\ nm$. Reproduced from Ref. [22].

2.4 Proof-of-principle experiments in microwave regime

Knowing the difficulties in fabricating the proposed optical TCMs, we performed proof-of-concept experiments in microwave regime to verify the idea. In microwaves, metals behave as perfect conductors and do not exhibit finite negative ε. However, metallic meshes with subwavelength openings are shown to exhibit Drude-like ε in microwave regime [32], and therefore, we designed mesh-based MTMs to mimic the plasmonic metals B and C at optical frequencies. In our designs, the unit air-hole is a $2.5\times15.5\ \text{mm}^2$ rectangle in mesh B and is a $3.5\times3.5\ \text{mm}^2$ square in mesh C, and each metallic line is 0.5 *mm*-wide and 0.05 *mm*-thick. Mesh B was put on a 0.6 *mm*-thick substrate with $\varepsilon_A = 5$, and mesh C was sandwiched between two such substrates. We fabricated realistic B and C samples [see insets to Figs. 5(a)-(b) for pictures], and measured their transmission spectra. Figures 5(a)-(b) show that the measured spectra are in excellent agreement with FEM simulations. From the calculated spectra, we derived the effective permittivity of the two materials as $\varepsilon_B = 5 - 580/f^2$ and $\varepsilon_C = 5 - 2300/f^2$, with f denoting linear frequency measured in *GHz*. At $f \sim 4.5\ GHz$, we have $\varepsilon_C \approx -109$, $\varepsilon_B \approx -24$ indicating that our MTMs can indeed well mimic plasmonic metals in optical regime.

With materials C and B both available, we choose the substrate as material A, cut A and B layers to stripes with $w_A = 1$ mm and $w_B = 3$ mm, and then construct an ABC structure based on the design shown in Fig. 3(a). Here we set $h_a = 1mm$ after optimizations. Figure 5(c) depicts the measured and simulated transmission spectra through such an ABC structure, where a transparent band is identified at ~4.4 *GHz* with peak *T* ~100%! This is quite counter-intuitive at first glance, since a bare layer C is nearly opaque here (with T < 5%). However, by adjusting the AB configuration based on Eqs. (3-4), we can make the scatterings from the two AB layers strong enough to perfectly cancel the scattering by the C layer alone, leading to perfect transparency of the whole structure.

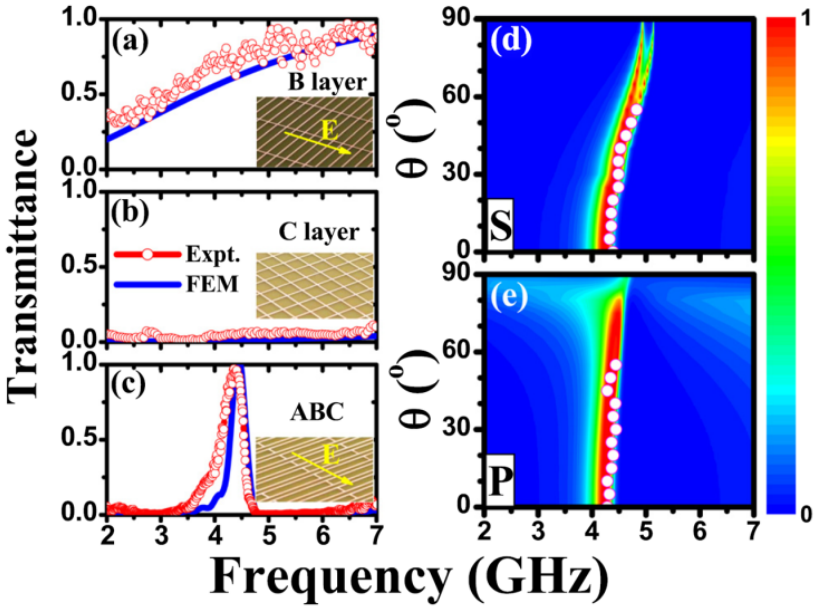

Fig. 5 (color online) Measured (open circles) and simulated (solid lines) transmission spectra of (a) layer B, (b) layer C, and (c) the designed ABC structure. FEM-calculated transmittance as functions of incident angle and frequency for (d) *S*- and (e) *P*-polarized incident waves, with open circles representing the measured maximum-transmittance positions. Reproduced from Ref. [22].

The discovered transparency possesses several attractive properties. Shown in Figs. 5(d)-(e) are the simulated T versus incidence angle θ and frequency *f* of the input EM waves with S- (keeping $\vec{E} \| \hat{x}$) or P-polarizations (keeping $\vec{H} \| \hat{y}$). Experimental data of peak-*T* positions are denoted as open circles in the same figures. Clearly, our transparency is rather stable against varying θ. Meanwhile, our scheme is also insensitive to structural disorder. We purposely re-designed and fabricated the AB layers to let w_A randomly located within $1.0 \times (1 \pm 10\%)$ mm and measured the transmission spectrum through such a disordered ABC structure. Figure 6(a) shows that the transparency is still there. As a comparison, we also designed and fabricated microwave samples that can support EOT-like transparency (upper high-T band in Fig. 3) at a similar frequency. Both experiments and simulations show that, while

the peak T for a perfectly ordered sample can be as large as 80% (see Fig. 6(b)), such an EOT transparency is almost killed when the same structural randomness is imposed, as shown in Fig. 6(c).

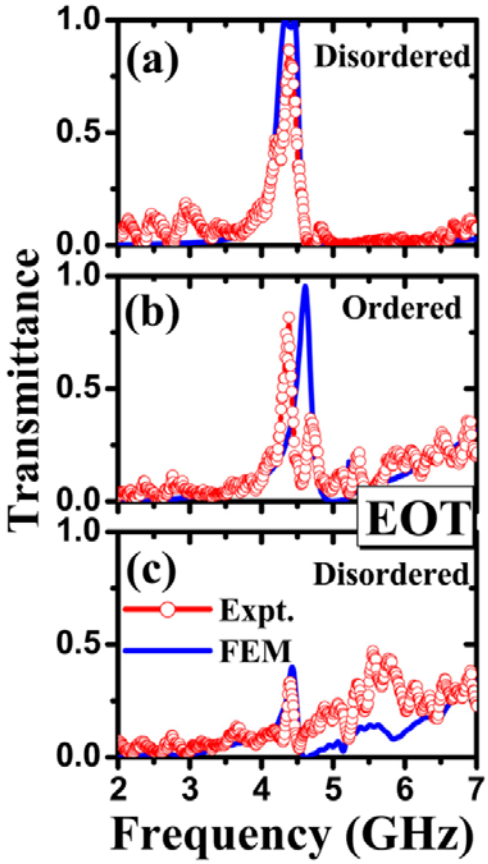

Fig. 6 (color online) Measured (open circles) and simulated (solid lines) transmission spectra of (a) a disordered ABC structure supporting the SCM transparency and (b, c) two designed structures supporting EOT-like transparencies. Here, the AB-stripes arrangement is perfectly ordered in (b) and is disordered in (a) and (c). Reproduced from Ref. [22].

2.5 TCMs on substrates: concept and realization in THz regime

In previous subsections, our efforts have been devoted to making free-standing TCMs. However, in many real applications such as solar cells, the TCMs should be deposited on a substrate. In this case, the substrate itself having a high refractive index may induce substantial reflections, which should be avoided in applications. Therefore, it is highly desired to consider such a more realistic geometry in designing TCMs.

In 2012, we extended the SCM for free-standing geometry to this on-substrate geometry [33]. As illustrated in Fig. 7(a), our theoretical model comprises a layer of the targeted metal film (named layer C) with permittivity ε_C on top of a semi-infinite substrate and another layer

consisting of alternate A and B strips (named layer AB). The width of the strips A and B are respectively denoted by w_A and w_B, and the periodicity of layer AB is $P = w_A + w_B$. Meanwhile, the thicknesses of layers AB and C are respectively d_{AB} and d_C.

Suppose that the y-polarized light at a specified wavelength illuminates the structure at normal incidence. Numerical simulations were performed based on FEM [23] to investigate the dependence of *T* (through the interface between C and substrate) on ε_B and P/λ. The results are depicted in Fig. 7(b) with all other parameters fixed as: $\varepsilon_A = \varepsilon_{sub} = 12,\ \varepsilon_C = -40,\ w_B = 0.1\lambda_0,\ d_{AB} = d_C = 0.02\lambda_0$, where λ_0 is the incident wavelength in free space. Since w_B is unchanged, varying w_A means the corresponding variation of P at a specified incident wavelength λ_0. According to the phase diagram, we find that the entire system becomes nearly perfectly transparent when the geometrical and material parameters satisfy certain conditions, although a standing-alone C layer on substrate only has a transmittance ~20%.

The discovered phenomenon can be explained by the SCM in the same spirits as in Ref. [17, 22]. Since $P << \lambda_0$, the composite AB layer can be homogenized based on EMT [18]. In the long wavelength limit, the effective permittivity of the AB layer, for the y-polarized wave, can be obtained by:

$$\frac{1}{\varepsilon_{AB}} = \frac{1}{\varepsilon_A}\frac{w_A}{P} + \frac{1}{\varepsilon_B}\frac{w_B}{P}, \tag{7}$$

Then we employed transfer matrix method (TMM) [19] to analytically calculate the reflection coefficient of the interface between C and substrate, $r = -Q_{21}/Q_{22}$. Obviously, perfect transparency in the ideal lossless system is obtained in the case of $|Q_{21}| = 0$. Therefore, analysis of Q_{21} will give us the directions for realizing transparency. After some tedious calculations, we got

$$\begin{aligned} Q_{21} = &\left[(1 - \frac{1}{\sqrt{\varepsilon_{sub}}}) \right] + i \times \left[(\frac{1}{\sqrt{|\varepsilon_C|}} + \frac{\sqrt{|\varepsilon_C|}}{\sqrt{\varepsilon_{sub}}}) \tanh(\sqrt{|\varepsilon_C|} d_C / \lambda_0) \right] \\ &+ i \times \left[(\frac{1}{\sqrt{\varepsilon_{AB}}} - \frac{\sqrt{\varepsilon_{AB}}}{\sqrt{\varepsilon_{sub}}}) \tan(\sqrt{\varepsilon_{AB}} d_{AB} / \lambda_0) \right] \\ &- (\frac{\sqrt{\varepsilon_{AB}}}{\sqrt{|\varepsilon_C|}} + \frac{\sqrt{|\varepsilon_C|}}{\sqrt{\varepsilon_{AB}}\sqrt{\varepsilon_{sub}}}) \tan(\sqrt{\varepsilon_{AB}} d_{AB} / \lambda_0) \tanh(\sqrt{|\varepsilon_C|} d_C / \lambda_0) \end{aligned} \tag{8}$$

We note that all terms in Eq. (9) have clear physical interpretations. The first two terms represent scatterings from the semi-infinite substrate and the C layer, respectively. The third term is clearly contributed by the AB layer. Finally the forth term results from multiple scattering in all layers. It is obvious from Eq. (9) that the presence of the AB layer can generate additional scattering terms (the last two ones) to cancel those contributed by the C layer and the semi-infinite substrate. From the view of mathematics, the minimized quantity $\left|Q_{21}/Q_{22}\right|$ is a crucial point in Eq. (9) for transmission as high as possible. The solutions obtained by the minimization procedure are depicted in Fig. 7(b) with the open circles. We find the FEM simulated transparency bands match quite well with the minimization model results, indicating that the present discovered transparency is indeed governed by the SCM.

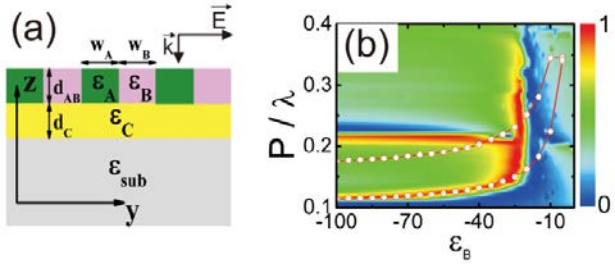

Fig. 7 (color online) (a) Schematic illustration of the proposed structure. (b) Transmission (colorful scale) as the function of ε_B and P/λ with all other parameters fixed. Open circles are obtained by minimizing $\left|Q_{21}/Q_{22}\right|$. Reproduced from Ref. [32].

The discrepancies between full-wave simulations and model results are found mainly for the upper branch and in the right part of the graph. It is easily understandable since in these regions the structure cannot be considered deeply sub-wavelength, so that the effective medium description of the AB layer is not accurate anymore. It is interesting to note that, while the effective medium model considerations do not guarantee the existence of perfect transparency, the full-wave simulations on realistic structures show that the maximized transmission in each case can indeed be almost 100%.

In principle, our concept can be applicable to any EM frequency domain as long as the required material parameters can be realized. Here we choose the THz domain to verify the concept experimentally. Similar to the microwave realizations, we exploited sub-wavelength metallic meshes [32] as plasmonic-like MTMs to achieve effectively negative permittivity in THz regime. The unit cell of the C layer shown in bottom one of Fig. 8(a) is a $4\,\mu m$ line-width metallic mesh with periodically arranged $46\,\mu m \times 46\,\mu m$ air squares and a lattice constant of $50\,\mu m$. The B metallic mesh is a $100\,\mu m \times 30\,\mu m$ rectangular. The vertical cross-section of the sample is shown in Fig. 8(b). The semi-infinite substrate is assumed as Si with $\varepsilon_{Si} = 11.7$, the $12\,\mu m$-thick SiO_2 layer (with $\varepsilon_{SiO_2} = 3.85$ [34]) is considered as a spacer between the two metallic meshes and a 200 *nm*-thick SiO_2 layer is placed on the very top for protection.

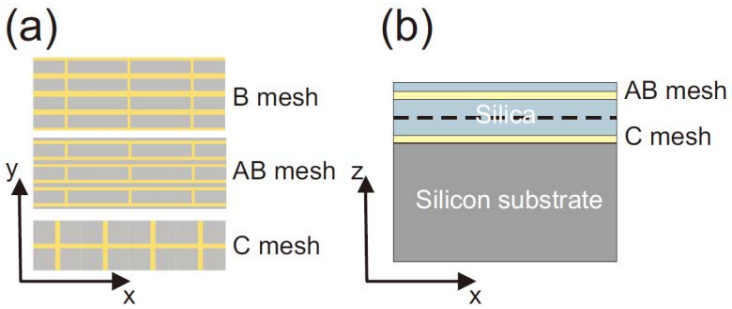

Fig. 8 (color online) the unit cells as seen from the xy plane (a) and the proposed structure in xz plane (b). The AB mesh is obtained by sectioning the B mesh and introducing a stripe of material, the A layer, in the cut. The dotted line represents the demarcation between the C and the AB MTM. Not on scale. Reproduced from Ref. [32].

In order to retrieve their effective permittivities, we first performed FEM simulations [23] to get the transmission spectra. Then we fitted the simulation results with the Drude model. It resulted that the permittivities of the MTMs B and C can be respectively described by $\varepsilon_B = 3.85 - (3.06/f)^2$ and $\varepsilon_C = 3.85 - (4.98/f)^2$, with f denoting the frequency in THz. For the f = 0.6 *THz*, these formulae give us $\varepsilon_C \sim -65$ and $\varepsilon_B \sim -22$, indicating that designed MTMs can indeed mimic plasmonic metals with the negative values of permittivity being in the desired range. The next step is to design the AB layer. The width of the A and B materials turns out to be $w_A = 10\ \mu m$ and $w_B = 30\ \mu m$. Through comparing the transmission spectra calculated with a homogeneous effective-medium slab and full-wave simulations on the realistic AB structure, we found that the effective permittivity of the AB layer can be given by $\varepsilon_{AB} = 3.85 + 4.19/(0.74^2 - f^2)$. The resonance behavior of ε_{AB} ensures that there must be a frequency where ε_{AB} exhibits the desired value to make the whole structure transparent. We successfully fabricated the THz samples based on the design and characterized their transmission/reflection properties. The measured results are in excellent agreement with simulation ones, as shown in Fig. 9.

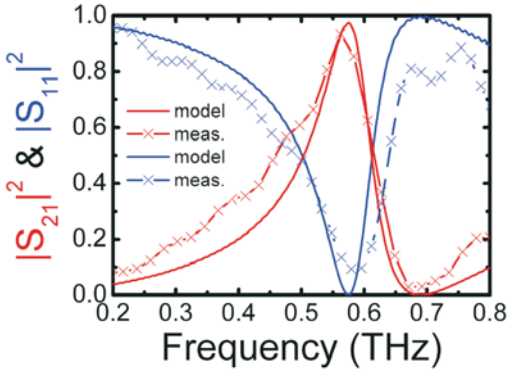

Fig. 9. (color online) Transmission and reflection data comparison. Full lines are the simulated results. The difference between the transmission max amplitude is mainly due to the difficulty in finding the optimum cutting point as well as neglecting the losses in the silica layer in simulations. Reproduced from Ref. [32].

Since our mechanism does not require any openings on the opaque metallic plate, the proposed structure retains the full electric and mechanical properties of a natural metal. This approach, demonstrated here for the THz regime, can be easily extended to other important frequency domains, e.g. the visible range, where demanding applications of transparent electrodes in photovoltaic cells, touch screens and other display devices exist. Although the design proposed here is only applicable to one particular in-plane E field polarization, it can be easily generalized to exhibit in-plane isotropic properties. We note that in 2010 Chen *et al.* suggested an approach for making anti-reflective coatings in THz regime [35], which can also be viewed as a mechanism to realize TCMs on substrates. However, our mechanism is more general and does not employ LC-resonant structures which suffer the saturation effect, and thus can be realized in optical frequency domain.

3. Inhomogeneous meta-surfaces for wave-front control

Manipulating EM waves as desired is the key motivation in MTM research. Historically, the designed/fabricated MTMs were either homogeneous or periodic. Recently, it was gradually realized that the macroscopic "order" of an MTM is another important degree of freedom that can be exploited to control EM waves. For example, based on recently developed transformation optics (TO) theory, MTMs with gradually changing properties have been designed to realize certain fascinating wave-manipulation phenomena, such as invisibility cloaking [5, 6] and optical illusions [36, 37]

Very recently, a class of inhomogeneous ultra-thin MTMs (also called meta-surfaces) attracted lots of attention [38-51]. These meta-surfaces were typically formed by planar meta-atoms with different and carefully designed EM responses, and employed the abrupt phase changes for waves passing through or reflected by the meta-surfaces to control the light wave-fronts. Compared to those TO media [5, 6, 36, 37], such meta-surfaces [38-51] suffer much less on the loss issue since EM waves do not propagate inside the medium for a long time.

In 2011, Capasso's group fabricated the first meta-surface based on V-shaped optical antennas working at $\lambda = 8\,\mu m$, and demonstrated several amazing light-manipulation effects [38]. The most remarkable discovery is that light reflection/refraction at a meta-surface with local transmission/reflection phase (denoted by Φ) linearly varying in space (i.e., $\Phi(x) = \Phi_0 + \xi x$) follows a general Snell's law,

$$k_{\parallel}^{'} = \xi + k_0 \sin\theta_i , \tag{10}$$

in which the parallel wave-vector is not conserved for reflected/transmitted wave, but rather

with an additional k vector compensated by the gradient ξ of the phase variation ($\xi = \nabla\Phi(x)$). Here $k_{\|}^{'}$ is the parallel wave-vector of the reflected or transmitted light, k_0 the free-space wavevector and θ_i the incident angle. Such a generalized Snell's law was independently derived in a different context by our group [39]. As shown in Fig. 10, as a gradient meta-surface is illuminated by a normal incident light, different parts of the system may response with different phase delays so that the interference among waves radiated from the system leads to a reflected beam with a parallel wave-vector ξ. Figure 10(a) shows an ideal realization of the meta-surface with continuously varying material properties, but more frequently such a system is formed by carefully selected meta-atoms (see Fig. 10(b)).

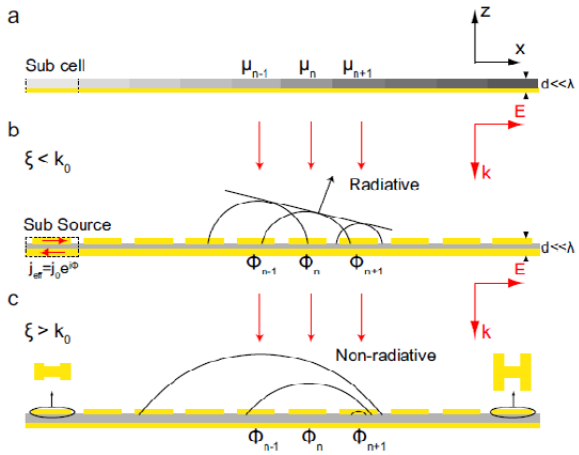

Fig. 10 (color online) (a) Effective-medium model of the gradient meta-surface system. Under illuminations of a normally incident PW, schematic pictures showing the radiation processes for realistic gradient meta-surfaces with (b) $\xi < k_0$ and (c) $\xi > k_0$. Reproduced from Ref. [39].

Capasso's group employed far-field measurements to experimentally verify the generalized Snell's law for different incident angles [38], based on their V-shaped meta-surfaces working on $8\ \mu m$. Shortly after this work, Shalaev's group pushed the idea to a shorter wavelength (~$2\ \mu m$) by down scaling the antenna's size, and demonstrated that the functionality of such a device is rather broadband [40]. However, these meta-surfaces share one common drawback that the efficiencies of anomalous reflection/transmission are very low (2%～5%) [38, 40]. This is because these devices support not only anomalous reflection/transmission modes, but also normal refraction/transmission modes. Another drawback is that the generated anomalous modes take different polarization as the incident one, since these systems utilized the bi-anisotropic response of the V-shaped antenna.

In 2012, our group proposed a new type of meta-surface and demonstrated that such meta-surfaces can overcome the shortcomings of previous designs [39]. As shown in Fig. 11, the building block of our meta-surface is a sandwich structure consisting of resonant metallic "H" and a continuous metal sheet, separated by a dielectric spacer. Thanks to the metallic substrate on the back, these meta-surfaces do not allow transmissions and suppress almost completely the

normal (specular) mode, so that the efficiency for anomalous reflection is nearly 100%. Figures 11(d)-(f) depict the measured scattering patterns of meta-surfaces with different ξ, when illuminated by normal incident microwaves. In addition to the apparent improvement in efficiency problem (see Fig. 11), we pushed the concept of generalized Snell's law significantly forward by showing that the incident propagating wave (PW) can be converted to surface waves (SW), when $\xi > k_0$ or the incident angle is larger than a critical value. The concept of PW-SW conversion can be understood from Fig. 10(c). When the phase gradient ξ is larger than k_0, the interferences among those waves radiated from different local parts of the meta-surface can not form a PW leaving the surface, but rather form a SW bounded on the surface. As a result, the far-field measurement failed to collect any signal for such a meta-surface (see Fig. 11(h)). We employed near-field scanning experiment to characterize such a PW-SW conversion and found that indeed a well-defined SW with $k_x = \xi$ is formed on the meta-surface, which also explained why the far-field measurement can not receive any radiation waves. We further demonstrated that such SW can be guided out of the meta-surface to flow as SPP on another system supporting an eigen SPP mode [39].

The idea we soon pushed to optical frequency [41], where conversion efficiency as high as 80% was demonstrated for anomalous reflections based on an optical meta-surface working around ~850 *nm*. Employing similar ideas, many other interesting wave-manipulation effects were explored based on modulating the reflection/transmission phase distribution, including aberration free lenses and axicons [42], optical vortex plate [43], out-of-plane wave reflector [44], broad-band wave plates [45], planar lenses [46], etc., realized in different frequency domains.

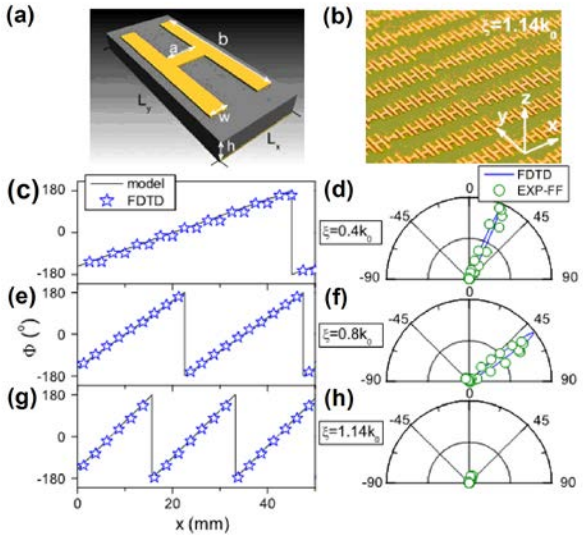

Fig. 11 (color online) (a) Geometry of a unit cell of the gradient meta-surface: a metallic H and a metal plate separated by a dielectric spacer ($\varepsilon_r = 3.9$). (b) Picture of part of fabricated $\xi = 1.14\,k_0$ sample. (c), (d) and (e) are reflection phase distributions, $\Phi(x)$, and (f), (g), (h) are measured and simulated scattering patterns for three meta-surfaces with $\xi / k_0 = 0.4$, 0.8 ,1.14 . Reproduced from Ref. [39].

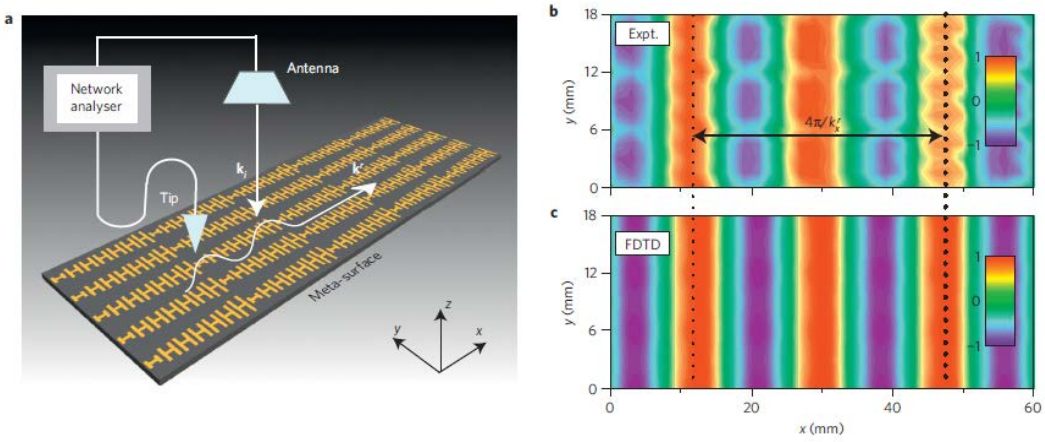

Fig. 12 (color online) (a) Schematic picture of the near field scanning technique. (b) Experimentally measured and (c) simulated E_z distributions (with phase information included) on part of the $\xi = 1.14k_0$ meta-surface under illumination of a normally incident x-polarized EM wave. Reproduced from Ref. [39].

In all those meta-surfaces mentioned above, the $\Phi(x)$ profiles were controlled by changing the geometrical size of each building block. Recently, several groups experimentally demonstrated that one could manipulate the reflection/transmission phase for circularly polarized (CP) waves through rotating the orientation of identical building block forming the meta-surface [47]. Such a phase is called Pancharatnam−Berry (PB) phase which has a profound geometrical origin [48, 49]. This idea opens a new route to manipulate the local phases, based on which many novel effects for manipulating CP lights are presented, such as anomalous reflection/transmission [47], optical vortex plate [47], ultra-thin flat lenses [50], and PW-SPP converter [51].

4. Conclusions

To summarize, we present a short overview on two hot topics in MTM field, focusing mainly on those works done in our own group. We follow the logical line of concept - realization - application to review the developments of these two sub-fields. Based on the concept of scattering cancellation, we show that a continuous plasmonic metal, either standing alone or put on a semi-infinite substrate, can be made optically transparent. The most attractive advantage of this scheme is that the target metal is continuous and thus keeps its high conductivity. We experimentally prove this concept in both microwave and THz frequency domains, based on different geometries. We also summarize the key developments so far achieved in the booming field of meta-surface. We show that Snell's law can be generalized at a carefully designed meta-surface with laterally modulated reflection/transmission phase profile, and such a system can even perfectly convert an impinging propagating wave to a surface wave under certain conditions. We have introduced the available efforts of realizing these amazing effects in different frequency domains, and several interesting applications of such devices. After more

than 10 years' development, MTMs continue to give us surprises, in both matured fields such as transparent metals or in the emerging fields such as meta-surfaces. We are looking forward to more fascinating new ideas and new developments in these fields.

References

[1] V. G. Veselago. "The Electrodynamics of Substances with Simultaneously Negative Value of ε and μ". *Sov. Phys. Usp.*, 10, 509-514 (1968).

[2] R. A. Shelby, D. R. Smith, and S. Schultz. "Experimental Verification of a Negative Index of Refraction". *Science*, 292, 77-79 (2001).

[3] J. B. Pendry. "Negative Refraction Makes a Perfect Lens". *Phys. Rev. Lett.*, 85, 3966-3969 (2000).

[4] N. Fang, H. Lee, C. Sun, et. al. "Sub–Diffraction-Limited Optical Imaging with a Silver Superlens". *Science*, 308, 534-537 (2005).

[5] U. Leonhardt. "Optical Conformal Mapping". *Science*, 312, 1777-1780 (2006).

[6] J. B. Pendry, D. Schurig, and D. R. Smith. "Controlling Electromagnetic Fields". *Science*, 312, 1780-1782 (2006).

[7] J. M. Hao, Y. Yuan, L. X. Ran, et. al. "Manipulating Electromagnetic Wave Polarizations by Anisotropic Metamaterials". *Phys. Rev. Lett.*, 99, 063908 (2007).

[8] J. M. Hao, Q. J. Ren, Z. H. An, et. al. "Optical metamaterial for polarization control". *Phys. Rev. A*, 80, 023807 (2009).

[9] T. Minami. "Present status of transparent conducting oxide thin-film development for Indium-Tin-Oxide (ITO) substitutes." *Thin Solid Films*, 516, 5822-5828 (2008).

[10] M. V. Exter and D. Grischkowsky. "Carrier dynamics of electrons and holes in moderately doped silicon". *Phys. Rev. B*, 41, 12140-12149 (1990).

[11] M. G. Kang, M. S. Kim, J. Kim, et. al. "Organic Solar Cells Using Nanoimprinted Transparent Metal Electrodes". *Adv. Mater.*, 20, 4408-4413 (2008).

[12] J. Y. Lee, S. T. Connor, Y. Cui, et. al. "Solution-Processed Metal Nanowire Mesh Transparent Electrodes". *Nano Lett.*, 8, 689-692 (2008).

[13] A. Boltasseva and H. A. Atwater. "Low-Loss Plasmonic Metamaterials". *Science*, 331, 290-291 (2011).

[14] D. R. Cairns, R. P. Witte, D. K. Sparacin, et. al. "Strain-dependent electrical resistance of tin-doped indium oxide on polymer substrates". *App. Phys. Lett.*, 76, 1425-1427 (2000).

[15] T. W. Ebbesen, H. J. Lezec, H. F. Ghaemi, et. al. “Extraordinary optical transmission through sub-wavelength hole arrays”. *Nature*, 391, 667-669 (1998).

[16] J. A. Porto, F. J. Garcia-Vidal, and J. B. Pendry. “Transmission resonances on metallic gratings with very narrow slits”. *Phys. Rev. Lett.*, 83, 2845-2848 (1999).

[17] L. Zhou,W. Wen, C. T. Chan, et. al. “Electromagnetic-Wave Tunneling Through Negative-Permittivity Media with High Magnetic Fields”. *Phys. Rev. Lett.*, 94, 243905 (2005).

[18] D. Bergman. “The dielectric constant of a composite material - a problem in classical physics”. *Phys. Rep.*, 43, 377-407 (1978).

[19] K. Busch, C. T. Chan, and C. M. Soukoulis. in *Photonic Band Gap Materials* edited by C. M. Soukoulis (Kluwer, Dordrecht, 1996) 16, 267-269 (1999).

[20] L. Zhou and C. T. Chan. “High-impedance reflectivity and surface-wave band gaps in metamaterials”. *Appl. Phys. Lett.*, 84, 1444-1446 (2004).

[21] J. Zhou, Th. Koschny, M. Kafesaki, et. al. “Saturation of the Magnetic Response of Split-Ring Resonators at Optical Frequencies”. *Phys. Rev. Lett.*, 95, 223902 (2005).

[22] Z. Y. Song, Q. He, S. Y. Xiao, et. al. “Making a continuous metal film transparent via scattering cancellations”. *Appl. Phys. Lett.*, 101, 181110 (2012).

[23] Comsol Multiphysics by COMSOL ©, ver. 3.5, network license (2008).

[24] F. J. Garcia-Vidal, L. Martin-Moreno, and J. B. Pendry. “Surfaces with holes in them: new plasmonic metamaterials”. *J. Opt. A: Pure Appl. Opt.*, 7, S97-S101 (2005).

[25] J. B. Pendry, L. Martin-Moreno, and F. J. Garcia-Vidal. “Mimicking Surface Plasmons with Structured Surfaces”. *Science*, 305, 847-848 (2004).

[26] I. El-Kady, M. M. Sigalas, R. Biswas, et. al. “Metallic photonic crystals at optical wavelengths”. *Phys. Rev. B*, 62, 15299-15302 (2000).

[27] G. Dolling, C. Enkrich, M. Wegener, et. al. “Low-loss negative-index metamaterial at telecommunication wavelengths”. *Opt. Lett.*, 31, 1800-1802 (2006).

[28] R. A . Paquin, Vol. II. Chap. 35 in *Handbook of Optics*, edited by M. Bass (McGraw-Hill, New York, 1995).

[29] N. Liu, M. Hentschel, T. Weiss, et. al. “Three-Dimensional Plasmon Rulers”. *Science*, 332, 1407-1410 (2011).

[30] J. M. Hao, J. Wang, X. L. Liu, et. al. “High performance optical absorber based on a plasmonic metamaterial”. *Appl. Phys. Lett.*, 96, 251104 (2010).

[31] J. M. Hao, C. W. Qiu, M. Qiu, a et. al. “Design of an ultrathin broadband transparent and high-conductive screen using plasmonic nanostructures”. *Opt. Lett.*, 37, 4955-4957 (2012).

[32] J. B. Pendry, A. J. Holden, W. J. Stewart, et. al. "Extremely low frequency plasmons in metallic mesostructures". *Phys. Rev. Lett.*, 76, 4773-4776 (1996).

[33] R. Malureanu, M. Zalkovskij, Z. Y. Song, et. al. "A new method for obtaining transparent electrodes". *Opt. Express*, 20, 22770-22782 (2012).

[34] M. Naftaly and R. E. Miles. "Terahertz time-domain spectroscopy of silicate glasses and the relationship to material properties". *J. Appl. Phys.*, 102, 043517 (2007).

[35] H. T. Chen, J. Zhou, J. F. OHara, et. al. "Antireflection coating using metamaterials and identification of its mechanism". *Phys. Rev. Lett.*, 105, 073901 (2010).

[36] Y. Lai, J. Ng, H. Y. Chen, et. al. "Illusion Optics: The Optical Transformation of an Object into Another Object". *Phys. Rev. Lett.*, 102, 253902 (2009).

[37] Y. Lai, J. Ng, H. Y. Chen, et. al. "Illusion optics". *Frontiers of Physics in China*, 5, 308-318 (2010).

[38] N. Yu, P. Genevet, M. A. Kats, et. al. "Light Propagation with Phase Discontinuities: Generalized Laws of Reflection and Refraction". *Science*, 334, 333-337 (2011).

[39] S. Sun, Q. He, S. Xiao, et. al. "Gradient-index meta-surface: A bridge linking propagating waves and surface waves". *Nat. Mater.* 11, 426-431 (2012).

[40] X. Ni, N. K. Emani, A. V. Kildishev, et. al. "Broadband Light Bending with Plasmonic Nanoantennas". *Science*, 335, 427, (2012).

[41] S. Sun, K. Y. Yang, C. M. Wang, et. al. "High-Efficiency Broadband Anomalous Reflection by Gradient Meta-Surfaces". *Nano Lett.*, 12, 6223-6229 (2012).

[42] F. Aieta, P. Genevet, M. A. Kats, et. al. "Dispersionless Phase Discontinuities for Controlling Light Propagation". *Nano Lett.*, 12, 5750-5755 (2012).

[43] P. Genevet, N. Yu, F. Aieta, et. al. "Ultra-thin plasmonic optical vortex plate based on phase discontinuities". *Appl. Phys. Lett.*, 100, 013101 (2012).

[44] F. Aieta, P. Genevet, N. Yu, et. al. "Aberration-Free Ultrathin Flat Lenses and Axicons at Telecom Wavelengths Based on Plasmonic Metasurfaces". *Nano Lett.*, 12, 1702-1706 (2012).

[45] N. Yu, F. Aieta, P. Genevet, et. al. "A Broadband, Background-Free Quarter-Wave Plate Based on Plasmonic Metasurfaces". *Nano Lett.*, 12, 6328-6333 (2012).

[46] X. Li, S. Xiao, B. Cai, et. al. "Flat metasurfaces to focus electromagnetic waves in reflection geometry". *Opt. Lett.*, 37, 4940-4942 (2012).

[47] L. Huang, X. Chen, H. Mühlenbernd, et. al. "Dispersionless Phase Discontinuities for Controlling Light Propagation". *Nano Lett.*, 12, 5750-5755 (2012).

[48] M. V. Berry. "The adiabatic phase and Pancharatnam's phase for polarized light". *J. Mod. Opt.*, 34, 1401-1407 (1987).

[49] S. Pancharatnam. "Generalized Theory of Interference, and Its Applications. Part I. Coherent Pencils". *Proc. Indian Acad. Sci. A* 44, 247-262 (1956).

[50] X. Chen, L. Huang, H. Mühlenbernd, et. al. "Dual-polarity plasmonic metalens for visible light". *Nat. Commun.*, 3, 1198 (2012).

[51] L. Huang, X. Chen, B. Bai, et. al. "Helicity Dependent Directional Surface Plasmon Polariton Excitation Using a Metasurface with Interfacial Phase Discontinuity". *Nature-Light: Science & Applications*, 2, e70 (2013).